Published in final edited form as:
J Neurosci. 2012 June 6; 32(23): 7941–7948. doi:10.1523/JNEUROSCI.0158-12.2012.

Acetylcholine receptor gating in a zebrafish model for slow channel syndrome

Michael Walogorsky[1], **Rebecca Mongeon**[1,2], **Hua Wen**[1], **Gail Mandel**[1,2], and **Paul Brehm**[1]

[1]Oregon Health & Science University, 3181 S.W. Sam Jackson Park Rd., Portland, Oregon, 97239

[2]Howard Hughes Medical Institute, 3181 S.W. Sam Jackson Park Rd., Portland, Oregon, 97239

Abstract

Slow channel syndrome (SCS) is an autosomal dominant disease resulting from mutations in muscle acetylcholine receptor (AChR) subunits. The associated fatigue and muscle degeneration are proposed to result from prolonged synaptic responses that overload intracellular calcium. Single channel studies on reconstituted receptors bearing human mutations indicate that the prolonged responses result from an increase in receptor open duration and, in some cases, increased sensitivity to acetylcholine (ACh). We show that both of these aberrant receptor properties are recapitulated in heterozygotic zebrafish bearing an L258P mutation in the α subunit, thus affording the unique opportunity to compare the single channel properties of mutant receptors to the synaptic currents *in vivo*. Whole cell recordings revealed synaptic currents that decayed along a multi-exponential time course, reflecting receptors containing mixtures of wild type and mutant α subunits. Treatment with quinidine, an open channel blocker used to treat the human disorder, restored fast synaptic current kinetics and the ability to swim. Quinidine block also revealed that mutant receptors generate a large steady state current in the absence of ACh. The spontaneous openings reflected a destabilization of the closed state, leading to an apparent increase in the sensitivity of these receptors to ACh. The effective block by quinidine on synaptic currents as well as non-liganded openings points to dual sources for the calcium-dependent myopathy in certain forms of SCS.

Keywords

Neuromuscular; myasthenic syndrome; congenital myasthenia; muscular dystrophy; quinidine

Introduction

Much understanding of SCS has emerged since the underlying mutations in muscle AChR subunits were first identified (Engel et al., 1993; Ohno et al., 1995). To date, mutations in α, β, δ and ε subunits have been reported, the majority of which are located near or within the pore forming regions (Ohno et al., 1995; Sine et al., 1995; Engel et al., 1996b; Gomez et al., 1996; Milone et al., 1997). Mutations in the γ subunit likely escaped detection because afflicted individuals recover during early development due to the switch from γ to the ε subunit. Most mutations are manifest as a destabilization of the closed state in favor of the open state, leading to prolonged channel openings (Ohno et al., 1995; Sine et al., 1995; Engel et al., 1996a; Gomez et al., 1996; Milone et al., 1997). This is causal to sustained

Corresponding Author: Paul Brehm, Vollum Institute, Oregon Health & Science University, 3181 S.W. Sam Jackson Park Rd., Portland, OR 97239, brehmp@ohsu.edu, Fax: 503-418-1624.

depolarizations, excessive calcium entry and postsynaptic degeneration (Engel et al., 1982; Gomez et al., 1997; Gomez et al., 2002). Single channel studies on muscle from patients (Engel et al., 1996b; Milone et al., 1997) and heterologously expressed channels bearing the relevant mutations (Sine et al., 1995; Engel et al., 1996b) point to two principal mechanisms causal to the stabilization of the open state. First, altered intrinsic channel gating that results in a slowed channel-closing rate. Second, an increased apparent affinity to ACh causal to re-openings by channels (Sine et al., 1995; Engel et al., 1996b; Milone et al., 1997).

Recordings of spontaneous synaptic currents from patients (Engel et al., 1982; Sine et al., 1995) and transgenic mice expressing a mutant ε subunit (Gomez et al., 1996), point to multiple kinetic components of synaptic decay as causal to prolongation. In the case of α subunit mutations, assignment of kinetic components to individual receptor isoforms is complicated by the presence of two copies in the receptor. Additionally, the γ and ε subunits compete for association with α, offering even greater potential for kinetic heterogeneity. Both of these sources apply to our zebrafish model for SCS, *twister*, which contains a point mutation in the acetylcholine receptor α subunit. We now capitalize on the advantages of this zebrafish model, wherein recordings of single channel currents and synaptic currents can be performed *in vivo* to identify the individual kinetic components. In particular, our ability to heterologously express defined wild type and mutant receptor isoforms enables assignment of the muscle counterparts.

Finally, for the first time, it was possible to test the functional effects of rescue by quinidine on *in vivo* synaptic currents. This long-lived open channel blocker is widely used to treat humans with SCS, based on the presumption that it accelerates synaptic current decay (Harper and Engel, 1998; Fukudome et al., 1998). We find that quinidine accelerated synaptic current decay but also showed an unexpected block of spontaneously open, non-liganded ACh receptors. Block of this standing source of depolarization and calcium entry likely represents an added restorative action by quinidine in patients afflicted with SCS.

Materials and Methods

Zebrafish (*Danio rerio*) were maintained in accordance with the standards set forth in the International Animal Care and Use Committee. The motility mutant *twister* line carries the formal nomenclature of *nic1*$^{\text{twister dbn12}}$ (Lefebvre et al., 2004), but for the purposes of the present study will be referred to as either twi$^{-/-}$ for homozygous carriers or twi$^{+/-}$ for heterozygous carriers. Animals of either sex were used for all experiments.

The methods used to record spontaneous synaptic currents and evoked synaptic currents were identical to those previously published (Mongeon et al., 2011). Synaptic currents were recorded using a HEKA Instruments EPC-10/2 amplifier (Instrutech Corp., Bellmore, NY) and 1μM tetrodotoxin was added for spontaneous synaptic current recordings. Synaptic currents were sampled at 10 μs and filtered at 5 kHz using Patchmaster software (Instrutech Corp., Bellmore, NY). Synaptic current decays of twi$^{+/-}$ were fit off-line to the sum of three exponential functions by Igor Pro (WaveMetrics, Lake Oswego, OR) using the Levenberg-Marquardt algorithm to search for the minimum chi square value. The fit required the entire peak to end range for proper estimation of all three exponential components. For both single channel and synaptic recordings the overall mean ± standard deviation was computed on the basis of the mean value for individual recordings. The *n* values refer to the number of recordings and the range of events used to compute the means are presented in the figure legends. The methods for paired motorneuron-muscle recording were identical to those previously published (Wen and Brehm, 2005).

Single channel recordings from fast skeletal muscle were made in the on-cell configuration using an Axopatch 200B amplifier (Molecular Devices, Sunnyvale, CA). The electrode and bath solutions were identical to those published previously (Mongeon et al., 2011). The muscle resting potential was estimated by adjusting the applied potential to eliminate all ACh activated single channel currents. Because the reversal potential of the ACh receptor is near 0 mV, this applied potential is taken as the muscle resting potential.

Single channel currents from zebrafish receptors heterologously expressed in *Xenopus* oocytes utilized the outside-out patch configuration as previously published (Mongeon et al., 2011). In these recordings the oocyte membrane potential was directly established and no corrections were required. Single channel records from both oocytes and muscle were acquired at 100 kHz and digitally filtered at 5 kHz. Individual channel events were detected based on half-amplitude tracking with TAC software (Bruxton Corporation, Seattle, WA) and events with burst durations < 200μs were excluded. The single channel burst duration and amplitude histograms were fit using TACfit software (Bruxton Corporation, Seattle, WA).

Macroscopic dose-response curves for applied agonists were performed using intact oocytes expressing specific receptor isoforms as previously described (Mongeon et al., 2011). The ACh was applied at a flow rate that resulted in complete exchange within 2 seconds. The dose-response curves for each isoform were fit by the Hill equation using IGOR Pro 5.05 (Paradiso and Brehm, 1998). Quinidine sulfate, choline chloride and d-tubocurare were all obtained from Sigma Chemical (St. Louis, MO) and made fresh in recording solution prior to each experiment. Alpha-bungarotoxin was obtained from Molecular Probes (Eugene, OR).

Fish movements were tracked at 1000 frames per second using a Fastcam 512-PCI camera (Photron Instruments, San Diego, CA) and were quantitated using Flote zebrafish behavioral analysis software (Burgess and Granato, 2007).

Results

Synaptic currents

The behavioral consequences of the L258P mutation are manifest as an inability of either of $twi^{-/-}$ or $twi^{+/-}$ fish to mount an effective swimming response during the first days of development (Lefebvre et al., 2004). Heterozygotic fish eventually recover the ability to swim but homozygotic fish exhibit a complete deterioration of muscle and death within the first few days of development. Consequently, $twi^{-/-}$ muscle cells are leaky and resistant to whole cell patch clamp. By contrast, $twi^{+/-}$ fish were healthy enough at all stages for patch clamp recordings. At 48 hpf, corresponding to the height of behavioral defect, the decay time course of mEPCs was greatly prolonged compared to those recorded from wild type muscle (Figure 1A). Fit of the current decay from $twi^{+/-}$ muscle generally required the sum of three exponential components termed the fast (τ_f), intermediate (τ_i), and slow (τ_s) time constants. The average time constants corresponded to 1.1 ± 0.3 ms, 8.6 ± 2.5 ms, and 70.2 ± 22.0 ms respectively (Figure 1A &B). This compares to 0.6 ± 0.3 ms for 48 hpf wild type fish, determined on the basis of a single exponential fit to the synaptic current decay. The average fractional contribution to overall peak synaptic current in $twi^{+/-}$ corresponded to 0.45 ± 0.09 for τ_f, 0.40 ± 0.09 for τ_i and 0.15 ± 0.08 for τ_s (Figure 1C).

The influence of the complex synaptic current kinetics on action potential generation was next determined using two approaches. First, simulated command-waveforms based on $twi^{+/-}$ and wild type synaptic current waveforms were injected directly into 48 hpf wild type muscle (Figure 2A & B). The current amplitudes were based on evoked synaptic currents

obtained using motorneuron-skeletal muscle paired recording. The decay time course was based on the mean time constants and fractional contribution by each exponential component. Under current clamp, both wild type and $twi^{+/-}$ synaptic waveforms consistently generated a single action potential (Figure 2A & B). Wild type repolarization was rapid compared to $twi^{+/-}$, which exhibited a prolonged after-depolarization. Next, muscle responses were recorded in paired motorneuron-muscle current clamp recordings (Figure 2C & D). The motorneuron action potentials were indistinguishable between $twi^{+/-}$ and wild type pairs and once again, only a single muscle action potential was observed, despite the greatly prolonged depolarization. Thus, both approaches point to a maintained contraction in $twi^{+/-}$ resulting from prolonged depolarization and not from repetitive firing of muscle action potentials.

Identifying the effects of the L258P mutation on gating of receptor isoforms

Recordings were made from zebrafish ACh receptors expressed in *Xenopus* oocytes in order to determine the effects of the α subunit mutation on single channel function. The oocytes were injected with RNA coding for the following combinations of zebrafish subunits: αβδγ, αβδε, α_{twi}βδγ or α_{twi}βδε. Prior to single channel recordings, dose-response relations to applied ACh were generated for whole oocytes expressing the different receptor isoforms. The relationships were then fit using the Hill equation and half maximum values were determined for each isoform (Figure 3). The average half-saturating concentrations for wild type αβδγ and αβδε receptors corresponded to 1.7 μM and 2.4 μM respectively. By contrast, the relationships for both receptor isoforms containing two α_{twi} subunits were shifted to lower concentrations. The mean half maximum corresponded to 12 nM for α_{twi}βδγ and 39 nM for α_{twi}βδε. Overall this reflects a 200-fold increase in apparent sensitivity to ACh for α_{twi}βδγ and a 44-fold increase for α_{twi}βδε.

Next, single channel currents from identified isoforms were recorded using outside-out oocyte patches from *Xenopus* oocytes. Visual inspection of sample traces for each of the four isoforms tested points to large differences in burst duration between wild type and mutant receptors (Figure 4A–D). Openings by both α_{twi}βδγ (Figure 4D) and α_{twi}βδε (Figure 4B) receptors were considerably longer than wild type αβδγ (Figure 4C) and αβδε (Figure 4A). Current-voltage relations obtained for both α_{twi}βδγ and α_{twi}βδε single channel currents were linear and yielded slope conductances of 48 pS and 60 pS respectively (Figure 4E). Both values were slightly lower than the αβδε and αβδγ counterparts (Figure 4F). The burst duration histograms for αβδε and α_{twi}βδε were each fit with a single exponential (Figure 4A & B) with overall mean time constants corresponding to 0.32 ± 0.05 ms and 9.27 ± 2.74 ms respectively. In the specific case of αβδε, the fast kinetics limited full resolution of the primary component of burst duration, so the mean time constant could potentially be even briefer than our estimate. The burst duration distribution for the αβδγ isoform required two exponentials for fit (Figure 4C). The predominant component for αβδγ corresponded to 0.67 ± 0.30 ms and contributed 75 ± 11% of total events whereas the minor slower component was 2.71 ± 1.10 ms and contributed 25 ± 11% of total events. The overall mean values for both wild type αβδε and αβδγ receptors were extracted from a large published database generated for reconstituted zebrafish receptors (Mongeon et al., 2011). The burst duration for the α_{twi}βδγ isoform was well fit by a single exponential with a mean value of 37.28± 12.66 ms, reflecting a 56-fold and 14-fold increase over the αβδγ fast and slow components respectively (Figure 4G).

Single channel counterparts in muscle

Single channel recordings of ACh-activated currents from $twi^{+/-}$ fast muscle were used to render assignment of the muscle receptors to specific receptor isoforms. Unfortunately, it was not possible to record ACh-activated currents from outside-out patches derived from

muscle so we turned to on-cell patch recordings. Recordings were first performed on twi$^{+/-}$ fish at 48 hpf, the time corresponding to the height of the motility defect and the analysis of synaptic current time course (Figure 5A). The electrode contained 300nM ACh in order to activate all of the isoforms present at this time. In three patches tested two amplitude classes could be observed with slope conductances of 44.1pS and 58.5 pS corresponding to γ and ε containing receptors respectively (Figure A & B). The cumulative burst duration histograms for the example in Figure 5C were complex and required three exponentials for fit with mean time constants corresponding to 0.5 ms, 3.4 ms and 44.8 ms. The individual burst components were next assigned to either ε or γ containing receptors by separating the event classes on the basis of amplitudes (Figure 5D &F). The burst duration for the large amplitude class was fit by two exponentials with time constants of 0.5 and 4.8 ms (Figure 5E). These time constants correspond to the αβδε and α_{twi}βδε receptors heterologously expressed in oocytes. The burst duration of the small amplitude class (Figure 5F) was also fit by two exponentials with time constants of 1.6 ms and 47.1 ms (Figure 5G), corresponding to the αβδγ and α_{twi}βδγ receptors isoforms.

Further confirmation of assignment was made by recording from 24 hpf muscle, a time when ε expression is expected to be low (Figure 6). The first recordings of ACh activated single channel currents came from twi$^{-/-}$ (Figure 6A–C). In these fish the α_{twi}βδγ isoform would be expected to be the predominant isoform. To maximize the openings at this early stage and minimize desensitization, the recordings were performed using 30nM ACh. In 7 recordings a single amplitude class was observed (Figure 6A & B) which corresponded to 44 pS (Figure 6J & K), which was similar to the 48 pS value measured for α_{twi}βδγ receptors. The open burst duration distribution for this class was well described by a single exponential function with time constant corresponding to 23.18 ± 3.92 ms (Figure 6C & L). Thus, on the basis of slope conductance and burst duration, this class corresponds to α_{twi}βδγ receptors. Recordings from twi$^{+/-}$ fish showed a class with similar amplitude (Figure 6D & E) and conductance (Figure 6J & K). The burst duration histogram was also fit by a single exponential (Figure 6F) with time constants similar to the homozygous fish (Figure 6L).

Confirmation of the high conductance class assignments was made using 120 hpf twi$^{+/-}$ fish where most receptors would be expected to contain the ε subunit. On cell recordings revealed a single amplitude class of openings (Figure 6G & H), with a slope conductance that corresponded to 62pS (Figure 6J & K). The burst duration of this class required two exponentials for fit with mean time constants corresponding to 0.41 ± 0.12 ms and 7.38 ± 1.86 ms (Figure 6I & L). These likely reflect mixed openings by α_{twi}βδε and αβδε receptors on the basis of conductance and burst duration.

Agonist and antagonist gating of mutant receptors

Alterations in the gating equilibrium were tested for possible involvement in heightened sensitivity to ACh for receptors harboring the *twister* mutation. First, we examined mutant receptors in the absence of ACh for evidence of non-liganded openings. Non-liganded openings were determined on the bases of both single channel and macroscopic current recordings from oocytes. In both cases the recording chamber was washed thoroughly to avoid lingering low concentrations of ACh. At the single channel level, non-liganded openings corresponding to either αβδε or αβδγ receptors were too rare to be annotated. By contrast, both α_{twi}βδγ and α_{twi}βδε receptors consistently showed single channel openings in outside-out patches in the absence of applied ACh. The frequency of the openings for α_{twi}βδγ however, was orders of magnitude greater (Figure 7A). The burst duration was brief in the absence of ACh compared to that seen in the presence of ACh, likely reflecting further stabilization of the open state in the presence of ACh (Figure 7A). The openings in

the absence of ACh points towards altered gating rather than altered binding as responsible for increased sensitivity to ACh (Jackson, 1984; Zhou et al., 1999).

Next, we searched for evidence of a macroscopic equivalent of non-liganded ACh receptor channel openings in oocytes expressing $\alpha_{twi}\beta\delta\gamma$ receptors. As a measure of non-liganded openings we tested two blockers of ACh receptors, the open channel blocker quinidine and the irreversible blocker alpha-bungarotoxin (α-btx). α-btx was tested at 1μM, while quinidine was tested at 100μM corresponding to 20 fold higher than used previously in single channel studies (Fukudome et al., 1998). This concentration was chosen in order to provide maximal block of spontaneous receptor openings by use of a slow channel blocker. In oocytes expressing either $\alpha\beta\delta\gamma$ or $\alpha\beta\delta\varepsilon$ receptors, neither agent had an effect on holding current (Figure 7C). By contrast, both agents led to large decreases in holding current in oocytes expressing $\alpha_{twi}\beta\delta\gamma$ receptors (Figure 7B & D). Pretreatment with α-btx eliminated the effects of quinidine, showing that the two agents were working through the same population of ACh receptors (Figure 7D). To estimate the fraction of total available ACh activated current contributed by spontaneous openings, we first determined the amplitude of quinidine sensitive holding current, then washed off the quinidine followed by treatment with 300 nM ACh to activate all available receptors (Figure 7B). The ratio of quinidine sensitive holding current to peak ACh activated current $\alpha_{twi}\beta\delta\gamma$ averaged 0.12 ± 0.07 (n=8; Figure 7C). This is remarkably high in light of the fact that the burst duration for spontaneous events is much briefer than in the presence of ACh (Figure 7A & B). Only small decreases in holding current were observed following quinidine treatment for $\alpha_{twi}\beta\delta\varepsilon$ receptors.

Next, choline, a very weak agonist of muscle nicotinic receptors, was tested for activation of mutant receptors (Figure 8A). Application of 1 mM choline to oocytes expressing wild type receptors resulted in weak fractional activations corresponding to 0.04 ± 0.01 for $\alpha\beta\delta\gamma$ and 0.03 ± 0.02 for $\alpha\beta\delta\varepsilon$ receptors (Figure 8A & B). By contrast, application of choline to either $\alpha_{twi}\beta\delta\gamma$ or $\alpha_{twi}\beta\delta\varepsilon$ receptor isoforms resulted in strong activation of inward current (Figure 8A & B). The fractional activation for $\alpha_{twi}\beta\delta\gamma$ and $\alpha_{twi}\beta\delta\varepsilon$ receptors corresponded to 0.92 ± 0.05 and 0.95 ± 0.04 both comparable to ACh activation (Figure 8B). The antagonist d-tubocurare was also tested for partial agonist action (Figure 8A). Application of 10 μM curare failed to significantly activate either $\alpha\beta\delta\gamma$ or $\alpha\beta\delta\varepsilon$ receptors (Figure 8B). However, significant responses were observed for both $\alpha_{twi}\beta\delta\gamma$ and $\alpha_{twi}\beta\delta\varepsilon$ receptor isoforms (Figure 8A & B). The mean fractional activation corresponded to 0.17 ± 0.08 for $\alpha_{twi}\beta\delta\gamma$ and 0.35 ± 0.09 for $\alpha_{twi}\beta\delta\varepsilon$ receptors (Figure 8B).

Quinidine effects on synaptic currents and non-liganded receptor openings

As quinidine is used for clinical treatment of patients afflicted with slow channel syndrome, we were prompted to directly test the effects on $twi^{+/-}$ fish. First, the effects on swimming were tested before and after treatment with quinidine (Figure 9A). As early as 48 hpf, wild type fish could generate alternating contractions as quantitated with motion tracking software (Figure 9A, top). At this age mutant fish were only able to generate a single maintained bend following mechanical stimulation (Figure 9A, bottom). To test for improvement, a high quinidine concentration of 50 μM was added to the bath solution for 10 minutes after which the fish were placed in a quinidine free bath solution for testing. The high concentration was used in order to facilitate entry into the live animal from the bath solution. In all, fish showed marked improvement in 7 of 10 testing groups in the ability to perform alternating contractions like those seen in wild type fish (Figure 9A). Next, we tested the effects of quinidine on synaptic currents. For this purpose mEPCs recorded from $twi^{+/-}$ fast muscle were compared before and after addition of 10 μM quinidine (Figure 9B). The mean amplitude of spontaneous synaptic currents was reduced, on average, by 45.9% in response to quinidine. However, the most pronounced effect of the treatment was a greatly

accelerated decay phase of the synaptic currents (Figure 9B). The triple exponential decay of synaptic currents in the $twi^{+/-}$ fish was converted to a decay that followed a single exponential time course with a mean time constant corresponding to 0.85 ± 0.40 ms (Figure 9B & C). There was no evidence of a slow or intermediate component of synaptic current decay at this concentration.

Discussion

Slow channel syndrome is a form of human congenital myasthenia associated with point mutations in the muscle nicotinic receptor subunits. Mutations in the α, β, δ and ε subunits have been identified, most of which are located in transmembrane domains (Ohno et al., 1995; Sine et al., 1995; Engel et al., 1996b; Gomez et al., 1996; Milone et al., 1997). Recordings from human biopsy muscle (Sine et al., 1995; Engel et al., 1996b), and transgenic mice over-expressing mutant subunits (Gomez et al., 1997; Gomez et al., 2002) have indicated prolonged synaptic potentials. However, the bulk of information regarding the functional consequences of individual mutations in humans has been extracted from single channel studies on mutated receptors. Overall, these measurements have pointed to a panel of functional alterations that are, to a large extent, shared by the different mutations. Topping the list are altered rate constants for channel gating that lead to prolonged channel openings, the presumed underpinnings of synaptic current prolongation (Sine et al., 1995; Engel et al., 1996b; Milone et al., 1997). Additionally, some of the mutations increase the sensitivity to ACh (Sine et al., 1995; Engel et al., 1996b; Milone et al., 1997) as well as alter the desensitization kinetics (Engel et al., 1996b; Milone et al., 1997). The common outcome of these functional alterations is enhanced receptor openings, leading to prolonged contractions and increased calcium overload.

The zebrafish mutant *twister* was identified through a dominant motility screen and mapped to an L258P mutation in the pore-lining M2 domain of the α subunit (Lefebvre et al., 2004). Recordings from $twi^{+/-}$ revealed greatly prolonged synaptic currents which result in a persistent depolarization. A single action potential accompanied the depolarization and subsequent firing was prevented until repolarization occurred. Because wild type synaptic currents result in spikes that repolarize quickly, they are able to follow frequencies in excess of 200 Hz (Wen & Brehm, 2005). These findings point to direct involvement of persistent depolarization as causal to the maintained contraction rather than persistent firing of action potentials.

Mutations in the α subunit differ from those in β, δ, ε and γ by virtue of two subunit copies in the same receptor. Consequently, in slow channel syndrome we would expect multiple functional receptor isoforms, attributable to mixtures of wild type and mutant α subunits. An additional layer of functional complexity is potentially introduced by the developmental switch between the γ and ε receptor isoforms (Mongeon et al., 2011). Due to the unique opportunity to perform *in vivo* recordings from $twi^{+/-}$ muscle, it was possible to resolve three kinetic components of the synaptic decay in $twi^{+/-}$. In order to assign synaptic components to individual receptor isoforms, we reconstituted both wild type and AChRs bearing the *twister* mutation in *Xenopus* oocytes to examine single receptor gating properties.

Single channel studies at 48 hpf formed the initial bases for assignment of the isoforms underlying individual components. At this stage both γ and ε isoforms were present, as reflected in the two conductance classes. The overall burst duration histogram required three exponential components for fit. The fast component fell within the mixed time constants for the αβδγ and αβδε receptors (Mongeon et al., 2012). The intermediate time constant was assigned to the high conductance isoform and corresponded to the $\alpha_{twi}\beta\delta\varepsilon$ whereas the slow

time constant was assigned to the low conductance isoform and corresponded to $\alpha_{twi}\beta\delta\gamma$. These assignments were further strengthened by recordings at 24 hpf where receptor isoforms were principally γ containing and 120 hpf where they were principally ε containing. While the slow component of synaptic current decay matches best the mean burst duration for the $\alpha_{twi}\beta\delta\gamma$ receptor, overall comparisons indicate a two-fold longer average for the decay. This difference is further reflected in single channel measurements from muscle at both 24 hpf and 48 hpf. This difference may reflect the reopening of receptors during the synaptic event. Reopening has been predicted to occur on the basis of the estimated rate constants for channel opening and ligand dissociation from single channel studies (Colquhoun and Hawkes, 1982, Sine and Steinbach, 1986). This may exacerbated by both the left shifted sensitivity of mutant receptors to ACh and/or by incomplete hydrolysis of ACh, a feature associated with early synapse development allowing rebinding by ACh and persistent re-opening of $\alpha_{twi}\beta\delta\gamma$ receptors (Kullberg et al., 1980; Nguyen et al., 1999; Drapeau et al., 2001).

In human SCS mutations, shifts in apparent affinity (Ohno et al., 1995; Engel et al., 1996b; Milone et al., 1997), the efficacy of weak agonists and competitive antagonists, (Milone et al., 1997) and spontaneous openings (Ohno et al., 1995; Engel et al., 1996b; Grosman and Auerbach, 2000) have all been reported. Such changes have been proposed to result from stabilization of the open state through changes in the di-liganded and non-liganded gating equilibrium constants. (Jackson 1984; Jackson 1986; Grosman and Auerbach, 2000). In the absence of agonist, wild type receptors have a low probability of opening because the closed conformation is energetically favored (Purohit and Auerbach, 2009; Auerbach, 2010). Reducing the free energy difference between the open and closed states increases the frequency of non-liganded spontaneous openings and shifts the midpoint of the dose response curve to lower concentrations. This allows a weak agonist, like choline, to effectively gate the receptor (Jadey et al., 2011).

Increased burst duration, spontaneous openings, enhanced sensitivity to ACh and gating by the weak agonist choline were all properties of receptors containing the mutant α subunit. Both $\alpha_{twi}\beta\delta\gamma$ and $\alpha_{twi}\beta\delta\varepsilon$ showed left shifted dose response curves and effective gating by choline. However, both burst duration and the frequency of spontaneous openings were much higher for the $\alpha_{twi}\beta\delta\gamma$ isoform pointing to differential interdependence of mutant α on ε versus γ subunit. For example, 30 nM ACh activates both short (αβδε-like) and long ($\alpha_{twi}\beta\delta\varepsilon$-like) burst duration components at 120 hpf in $twi^{+/-}$ fish. This low concentration would not be expected to activate wild type receptors. By contrast, at 24 hpf $twi^{+/-}$ there was no evidence of short (αβδγ–like) bursts at 30 nM ACh, only the very long $\alpha_{twi}\beta\delta\gamma$ bursts. This points to the possible existence of distinction between effects of mutant α on ACh sensitivity and gating when formed with the ε instead of the γ subunit. Our ability to draw firm conclusions about the receptor isoform and functional consequences is greatly compromised by the uncertainty surrounding receptors with a single mutant α subunit. Because receptors with two mutant α subunits can function, it is reasonable to surmise that receptors with single mutant subunits can function. However, we were unable to determine whether any or all of these functional properties are shared by receptors containing two mutant α subunits versus a single mutant α. The consequences may not be shared by receptors formed through association with the γ versus ε subunit. A second source of potential complication may relate to the position of a single mutant α subunit relative to the δ subunit. In other words, the interaction of mutant α may differ when partnered with δ than when partnered with either γ or ε,

Openings by the embryonic $\alpha_{twi}\beta\delta\gamma$ isoform are effectively blocked by quinidine. Quinidine is a long-lived open channel blocker used to treat humans afflicted with slow channel syndrome (Harper and Engel, 1998; Fukudome et al., 1998). Due to the technical

limitations involving human subjects, the effects on synaptic current have never been tested. The prediction that quinidine would serve as a channel blocker to accelerate synaptic current decay was based on the single channel studies. Our recordings provide the first measure of effectiveness, and substantiate the predicted effect. In response to 10 μM quinidine, the synaptic current decay time course shortened greatly, to the same extent seen for native adult wild type receptors. The decay of synaptic current is complete and shows no sign of incomplete block rendering it a powerful prophylactic treatment. Quinidine likely also carries a previously unappreciated source of treatment in the block of non-liganded spontaneous mutant receptor openings. For $\alpha_{twi}\beta\delta\gamma$ receptors, the non-liganded openings account for nearly 15% of the total available receptors. Such a large steady state current is predicted to outweigh the total integrated current associated with low frequency synaptic responses.

Finally, much evidence exists in support of long term postsynaptic deterioration in humans afflicted with slow channel syndrome (Milone et al., 1997; Engel et al., 1996b; Leonard and Salpeter, 1979; Leonard and Salpeter, 1982; Engel et al., 1982; Gomez et al., 1996; Gomez et al., 1997; Gomez et al., 2002) and has been directly linked to the calcium entering during the prolonged depolarization associated with synaptic currents (Gomez et al., 2002). Additional contributions by spontaneous receptor openings to postsynaptic degeneration were proposed for humans with slow channel syndrome (Engel et al., 1996b). So, as with human slow channel syndrome, there are two potential sources for calcium overload in $twi^{-/-}$ fish: prolonged synaptic current and spontaneous receptor openings. The fact that quinidine so effectively blocks both sources points to a dual role for this drug in preventing muscle degeneration resulting from calcium overload.

Acknowledgments

We thank Dr. David Dawson and Chris Alexander for generously providing *Xenopus* oocytes. Dr. Geng-Lin Li generated the multi-exponential fitting routine for synaptic current decay. Dr. Claudio Grosman helped greatly with our interpretation of spontaneous openings and altered agonist sensitivity. This work was supported by NIH grant NS18205 to P.B.

References

Auerbach A. The gating isomerization of neuromuscular acetylcholine receptors. J Physiol. 2010; 588:573–586. [PubMed: 19933754]

Burgess HA, Granato M. Modulation of locomotor activity in larval zebrafish during light adaptation. J Exp Biol. 2007; 210:2526–2539. [PubMed: 17601957]

Colquhoun D, Hawkes AG. On the stochastic properties of bursts of single ion channel openings and of clusters of bursts. Philosophical Transactions of the Royal Society London B. 1982; 300:1–59.

Drapeau P, Buss RR, Ali DW, Legendre P, Rotundo RL. Limits to the development of fast neuromuscular transmission in zebrafish. J Neurophysiol. 2001; 86:2951–2956. [PubMed: 11731551]

Engel AG, Hutchinson DO, Nakano S, Murphy L, Griggs RC, Gu Y, Hall ZW, Lindstrom J. Myasthenic syndromes attributed to mutations affecting the epsilon subunit of the acetylcholine receptor. Ann N Y Acad Sci. 1993; 681:496–508. [PubMed: 8357190]

Engel AG, Lambert EH, Mulder DM, Torres CF, Sahashi K, Bertorini TE, Whitaker JN. A newly recognized congenital myasthenic syndrome attributed to a prolonged open time of the acetylcholine-induced ion channel. Ann Neurol. 1982; 11:553–569. [PubMed: 6287911]

Engel AG, Ohno K, Bouzat C, Sine SM, Griggs RC. End-plate acetylcholine receptor deficiency due to nonsense mutations in the epsilon subunit. Ann Neurol. 1996a; 40:810–817. [PubMed: 8957026]

Engel AG, Ohno K, Milone M, Wang HL, Nakano S, Bouzat C, Pruitt JN 2nd, Hutchinson DO, Brengman JM, Bren N, Sieb JP, Sine SM. New mutations in acetylcholine receptor subunit genes

reveal heterogeneity in the slow-channel congenital myasthenic syndrome. Hum Mol Genet. 1996b; 5:1217–1227. [PubMed: 8872460]

Fukudome T, Ohno K, Brengman JM, Engel AG. AChR channel blockade by quinidine sulfate reduces channel open duration in the slow-channel congenital myasthenic syndrome. Ann N Y Acad Sci. 1998; 841:199–202. [PubMed: 9668240]

Gomez CM, Maselli R, Gammack J, Lasalde J, Tamamizu S, Cornblath DR, Lehar M, McNamee M, Kuncl RW. A beta-subunit mutation in the acetylcholine receptor channel gate causes severe slow-channel syndrome. Ann Neurol. 1996; 39:712–723. [PubMed: 8651643]

Gomez CM, Maselli R, Gundeck JE, Chao M, Day JW, Tamamizu S, Lasalde JA, McNamee M, Wollmann RL. Slow-channel transgenic mice: a model of postsynaptic organellar degeneration at the neuromuscular junction. J Neurosci. 1997; 17:4170–4179. [PubMed: 9151734]

Gomez CM, Maselli RA, Groshong J, Zayas R, Wollmann RL, Cens T, Charnet P. Active calcium accumulation underlies severe weakness in a panel of mice with slow-channel syndrome. J Neurosci. 2002; 22:6447–6457. [PubMed: 12151524]

Grosman C, Auerbach A. Kinetic, mechanistic, and structural aspects of unliganded gating of acetylcholine receptor channels: a single-channel study of second transmembrane segment 12' mutants. J Gen Physiol. 2000; 115:621–635. [PubMed: 10779319]

Harper CM, Engel AG. Quinidine sulfate therapy for the slow-channel congenital myasthenic syndrome. Ann Neurol. 1998; 43:480–484. [PubMed: 9546329]

Hoffmann K, Muller JS, Stricker S, Megarbane A, Rajab A, Lindner TH, Cohen M, Chouery E, Adaimy L, Ghanem I, Delague V, Boltshauser E, Talim B, Horvath R, Robinson PN, Lochmuller H, Hubner C, Mundlos S. Escobar syndrome is a prenatal myasthenia caused by disruption of the acetylcholine receptor fetal gamma subunit. Am J Hum Genet. 2006; 79:303–312. [PubMed: 16826520]

Jackson MB. Spontaneous openings of the acetylcholine receptor channel. Proc Natl Acad Sci U S A. 1984; 81:3901–3904. [PubMed: 6328531]

Jackson MB. Kinetics of unliganded acetylcholine receptor channel gating. Biophys J. 1986; 49:663–672. [PubMed: 2421793]

Jadey SV, Purohit P, Bruhova I, Gregg TM, Auerbach A. Design and control of acetylcholine receptor conformational change. Proc Natl Acad Sci U S A. 2011; 108:4328–4333. [PubMed: 21368211]

Kullberg RW, Mikelberg FS, Cohen MW. Contribution of cholinesterase to developmental decreases in the time course of synaptic potentials at an amphibian neuromuscular junction. Dev Biol. 1980; 75:255–267. [PubMed: 6245982]

Lefebvre JL, Ono F, Puglielli C, Seidner G, Franzini-Armstrong C, Brehm P, Granato M. Increased neuromuscular activity causes axonal defects and muscular degeneration. Development. 2004; 131:2605–2618. [PubMed: 15128655]

Leonard JP, Salpeter MM. Agonist-induced myopathy at the neuromuscular junction is mediated by calcium. J Cell Biol. 1979; 82:811–819. [PubMed: 511934]

Leonard JP, Salpeter MM. Calcium-mediated myopathy at neuromuscular junctions of normal and dystrophic muscle. Exp Neurol. 1982; 76:121–138. [PubMed: 6282613]

Milone M, Wang HL, Ohno K, Fukudome T, Pruitt JN, Bren N, Sine SM, Engel AG. Slow-channel myasthenic syndrome caused by enhanced activation, desensitization, and agonist binding affinity attributable to mutation in the M2 domain of the acetylcholine receptor alpha subunit. J Neurosci. 1997; 17:5651–5665. [PubMed: 9221765]

Mongeon R, Walogorsky M, Urban J, Mandel G, Ono F, Brehm P. An acetylcholine receptor lacking both gamma and epsilon subunits mediates transmission in zebrafish slow muscle synapses. J Gen Physiol. 2011; 138:353–366. [PubMed: 21844221]

Nguyen PV, Aniksztejn L, Catarsi S, Drapeau P. Maturation of neuromuscular transmission during early development in zebrafish. J Neurophysiol. 1999; 81:2852–2861. [PubMed: 10368402]

Ohno K, Hutchinson DO, Milone M, Brengman JM, Bouzat C, Sine SM, Engel AG. Congenital myasthenic syndrome caused by prolonged acetylcholine receptor channel openings due to a mutation in the M2 domain of the epsilon subunit. Proc Natl Acad Sci U S A. 1995; 92:758–762. [PubMed: 7531341]

Paradiso K, Brehm P. Long-term desensitization of nicotinic acetylcholine receptors is regulated via protein kinase A-mediated phosphorylation. J Neurosci. 1998; 18:9227–9237. [PubMed: 9801362]

Purohit P, Auerbach A. Unliganded gating of acetylcholine receptor channels. Proc Natl Acad Sci U S A. 2009; 106:115–120. [PubMed: 19114650]

Sine SM, Ohno K, Bouzat C, Auerbach A, Milone M, Pruitt JN, Engel AG. Mutation of the acetylcholine receptor alpha subunit causes a slow-channel myasthenic syndrome by enhancing agonist binding affinity. Neuron. 1995; 15:229–239. [PubMed: 7619526]

Sine SM, Steinbach JH. Activation of acetylcholine receptors on clonal mammalian BC3H-1 cells by low concentration of agonist. J. Physiol. 1986; 373:129–162. [PubMed: 2427693]

Wen H, Brehm P. Paired motor neuron-muscle recordings in zebrafish test the receptor blockade model for shaping synaptic current. J Neurosci. 2005; 25:8104–8111. [PubMed: 16135768]

Zhou M, Engel AG, Auerbach A. Serum choline activates mutant acetylcholine receptors that cause slow channel congenital myasthenic syndromes. Proc Natl Acad Sci U S A. 1999; 96:10466–10471. [PubMed: 10468632]

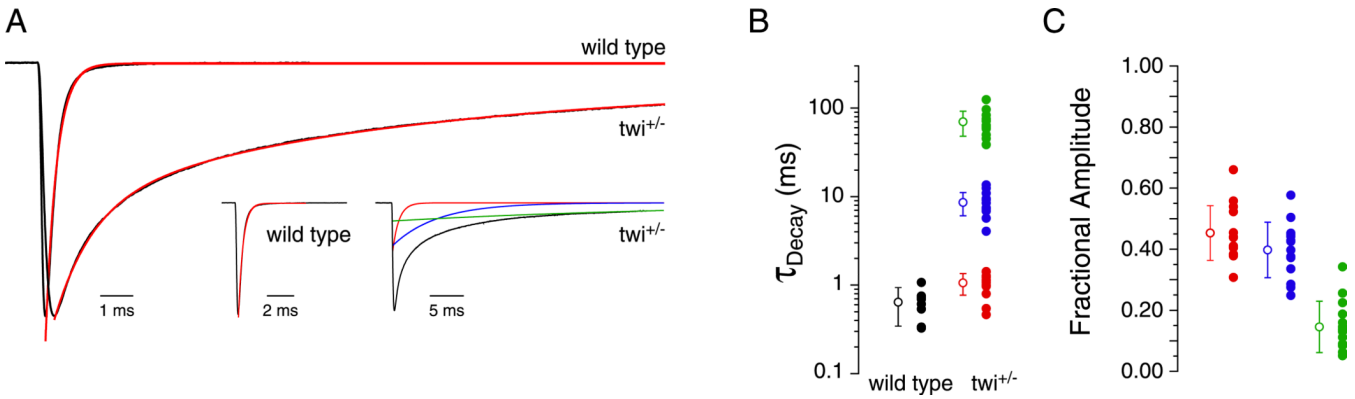

Figure 1. Kinetics of spontaneous endplate currents in wild type and twi$^{+/-}$ fast skeletal muscle

A, Representative mEPCs recorded from 48 hpf wild type and twi$^{+/-}$ fast muscle. Synaptic current decays (black) were fit peak-end (red overlay) by either a single exponential function for wild type or by the sum of 3 exponential functions for twi$^{+/-}$. The insets show the individual components of each fit. B, The mean decay time constants computed for each recording are indicated by filled circles and the overall mean ± SD by an open circle (wild type n=9, twi$^{+/-}$ n=14). Between 7 and 115 events were measured for each recording. C, Fractional contribution to overall amplitude by each exponential component in twi$^{+/-}$.

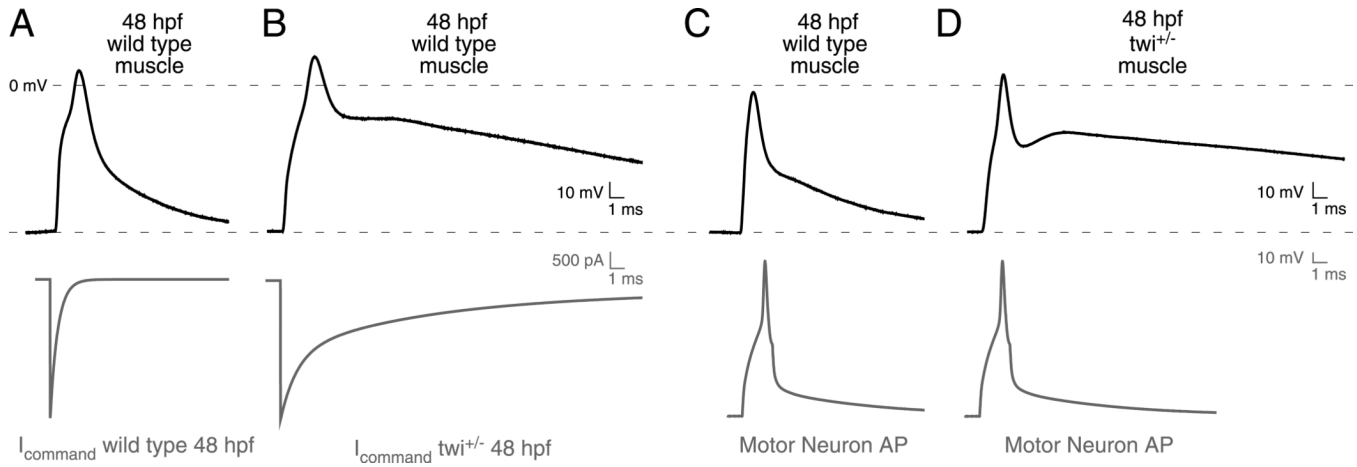

Figure 2. Effect of prolonged synaptic currents on post-synaptic potential

A,B, Representative action potential waveforms recorded from 48 hpf wild type fast muscle were elicited using voltage command waveforms based on the average synaptic current decays for wild type (A) and twi$^{+/-}$ (B) shown in Figure 1. The command waveforms are shown in red and the associated muscle responses are shown in black (n=5 cells; Between 12 and 20 action potentials were averaged for each cell). C,D, Paired current clamp recordings of motorneuron (red) and muscle action potentials (black) for 48hpf wild type (C; n= 4 pairs; 7–28 action potentials per cell) and twi$^{+/-}$ (D; n=6 pairs; 8–26 action potentials per cell) muscle.

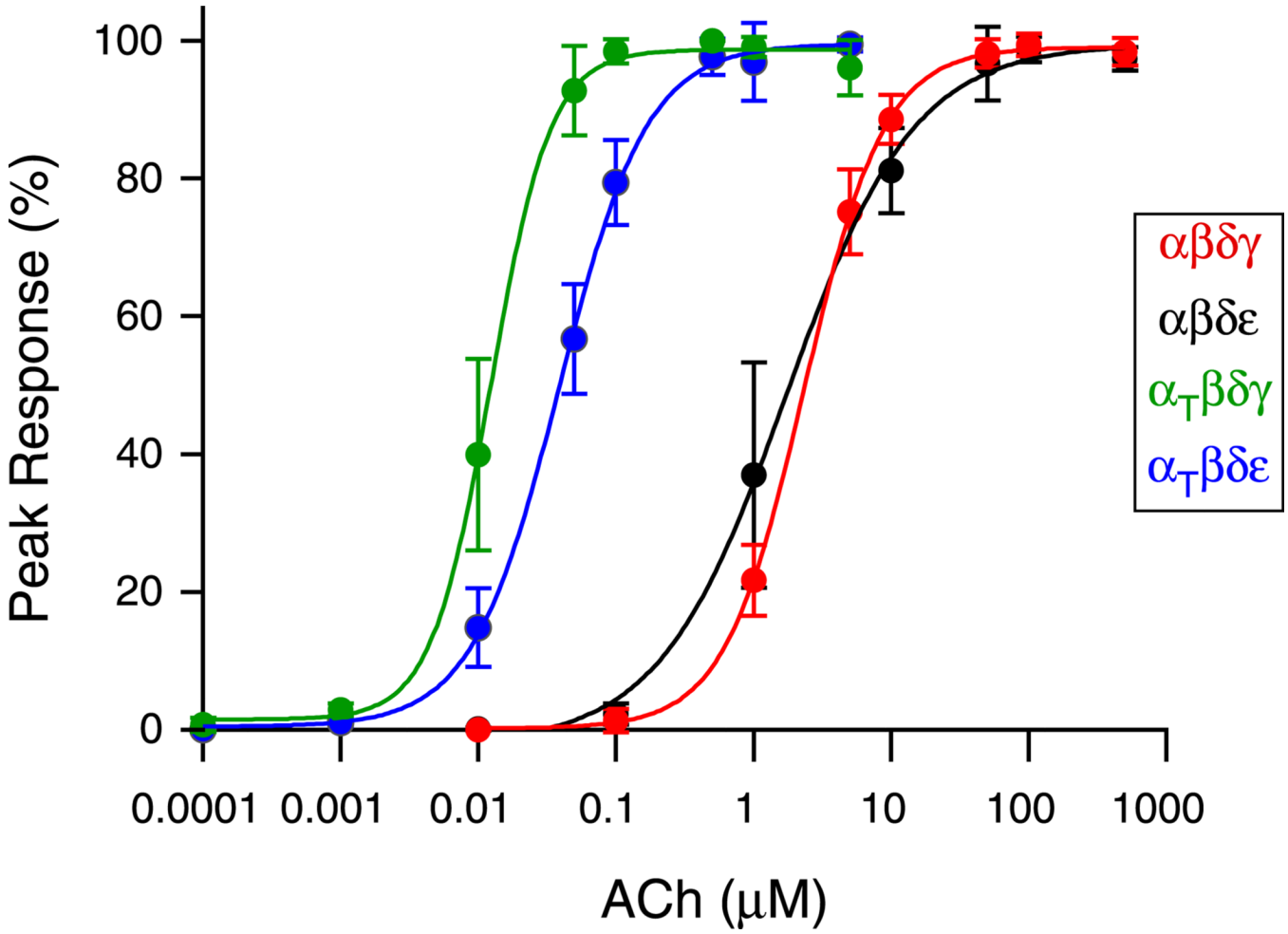

Figure 3. Dose response curves obtained for receptor subunit combinations expressed in *Xenopus* oocytes

Oocytes expressing either αβδγ (red), αβδε (black), α_{twi}βδγ (green) or α_{twi}βδε (blue) were voltage clamped at −50 mV and current responses to fast flow changes in ACh concentration were determined. Each point represents the mean ± SD of the percent of peak current determined for 6–7 oocytes at each ACh concentration. The dose-response relationships between peak ACh-activated current and ACh concentration were fit to the Hill equation $I = I_{max} / (1 + (K_{1/2}/[A])^n)$ where I is the current at a given concentration of agonist A, I_{max} is the peak ACh-activated current, $K_{1/2}$ is the half-maximal concentration, and n is the Hill coefficient.

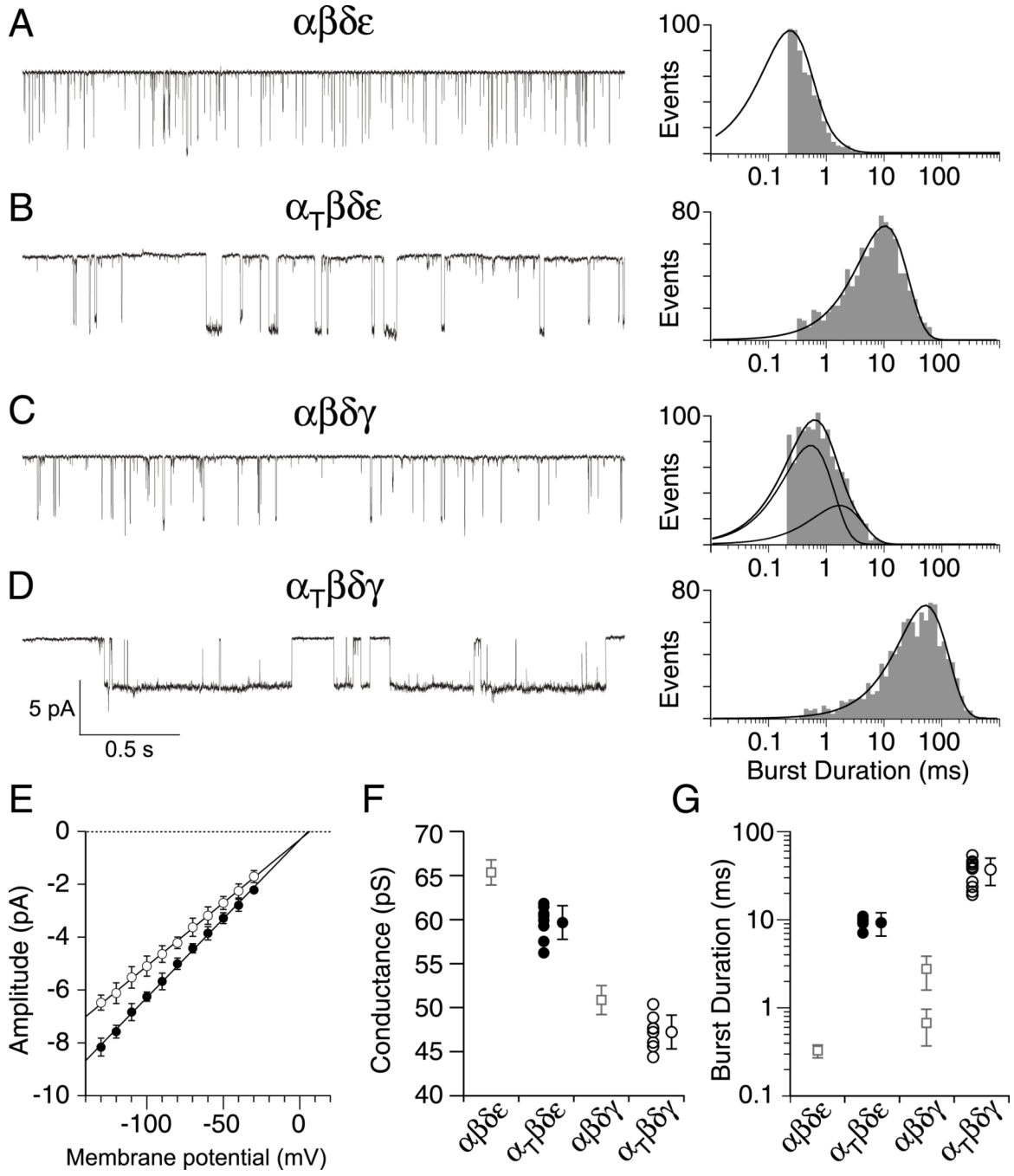

Figure 4. ACh-activated single-channel currents associated with different receptor isoforms

A–D, Representative single channel recordings of ACh activated currents from outside-out patches of *Xenopus* oocytes expressing either (A) αβδε (B) α_{twi}βδε (C) αβδγ or (D) α_{twi}βδγ receptors. Example semi-log burst duration histograms for each receptor isoform fit with either a single exponential (A, B & D) or bi-exponential (C) function. E, Cumulative current-voltage relations showing mean ± SD for α_{twi}βδε (filled circles, n=8 recordings) and α_{twi}βδγ (open circles, n=8 recordings) with linear fits. F, Scatterplot of mean slope conductances obtained for individual recordings from α_{twi}βδε (filled circles) and α_{twi}βδγ (open circles) shown alongside the overall mean ± SD for each distribution. The mean ± SD for wild type counterparts are shown as open squares (taken from Mongeon et al., 2011).

Between 31 and 111 events were used to generate each point in E and F. G, Scatterplot of mean burst duration from $\alpha_{twi}\beta\delta\varepsilon$ (filled circles, n=7 recordings) and $\alpha_{twi}\beta\delta\gamma$ (open circles, n=10 recordings) receptors along with the overall mean ± SD. Between 659 and 1147 events for each recording were used to generate the individual mean values. The wild type mean ± SD counterpart values are shown as open squares (taken from Mongeon et al., 2011).

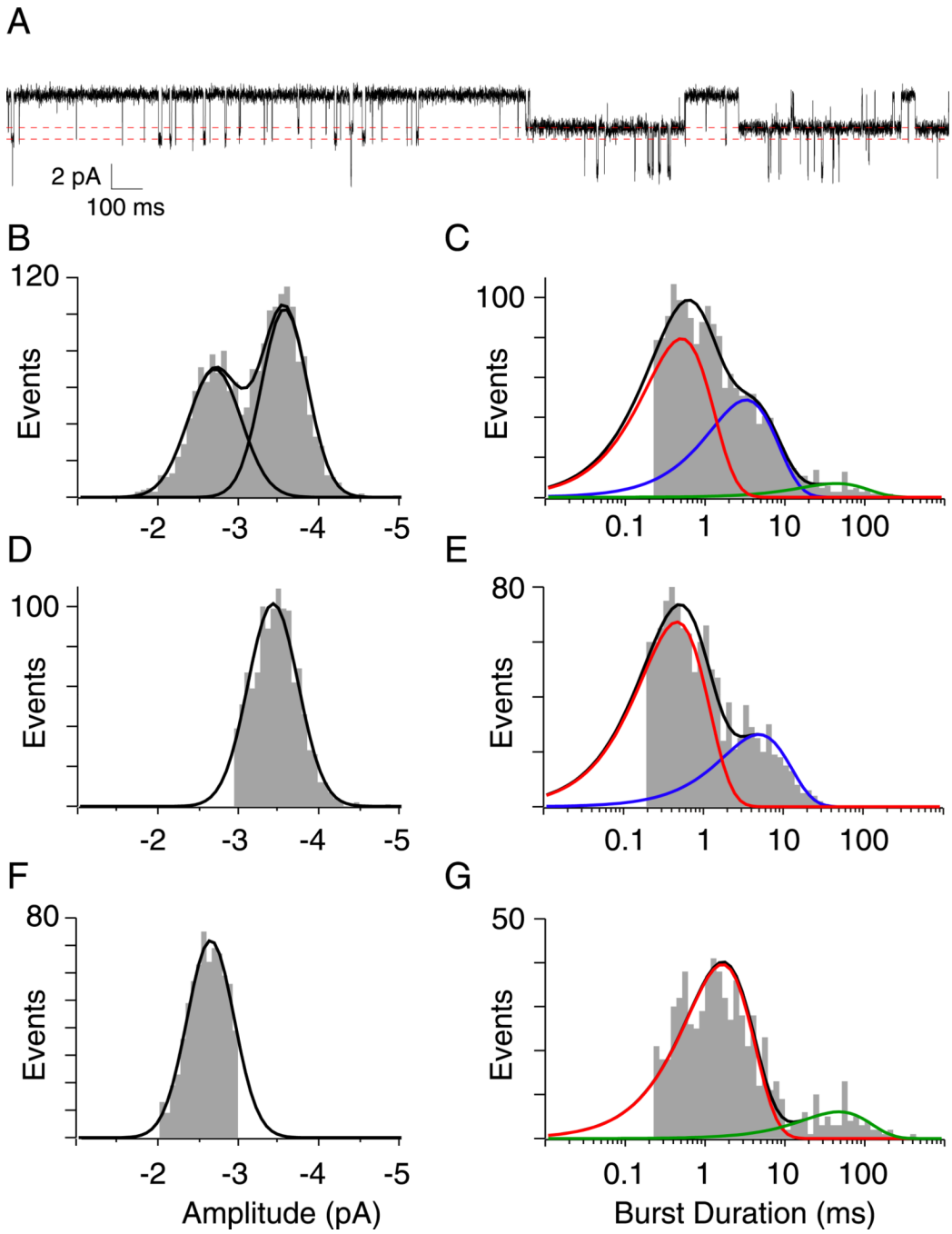

Figure 5. ACh activated single channel currents from 48hpf twi$^{+/-}$ fish

A, An ~3 second sample trace of channel openings to two amplitude levels in the presence of 300nM ACh. The dotted lines indicate the two open levels B, Amplitude histogram for all openings required the sum of two Gaussian distributions with means of −3.5 pA and −2.7 pA (n=1796 events) C, The burst duration histogram for all openings, fit to three exponential components with time constants corresponding to 0.5 ms, 3.4 ms and 44.8 ms. D, The distribution of large amplitude openings used to generate the burst duration in E (n=1065 events). E, The burst duration for large amplitude events was fit with two exponential components with time constants corresponding to 0.5 ms and 4.8 ms. F, The distribution of small amplitude openings used to generate the burst duration in G (n=731 events). G, The

burst duration for small amplitude events was fit with two exponential components with time constants corresponding to 1.6 ms and 47.1 ms.

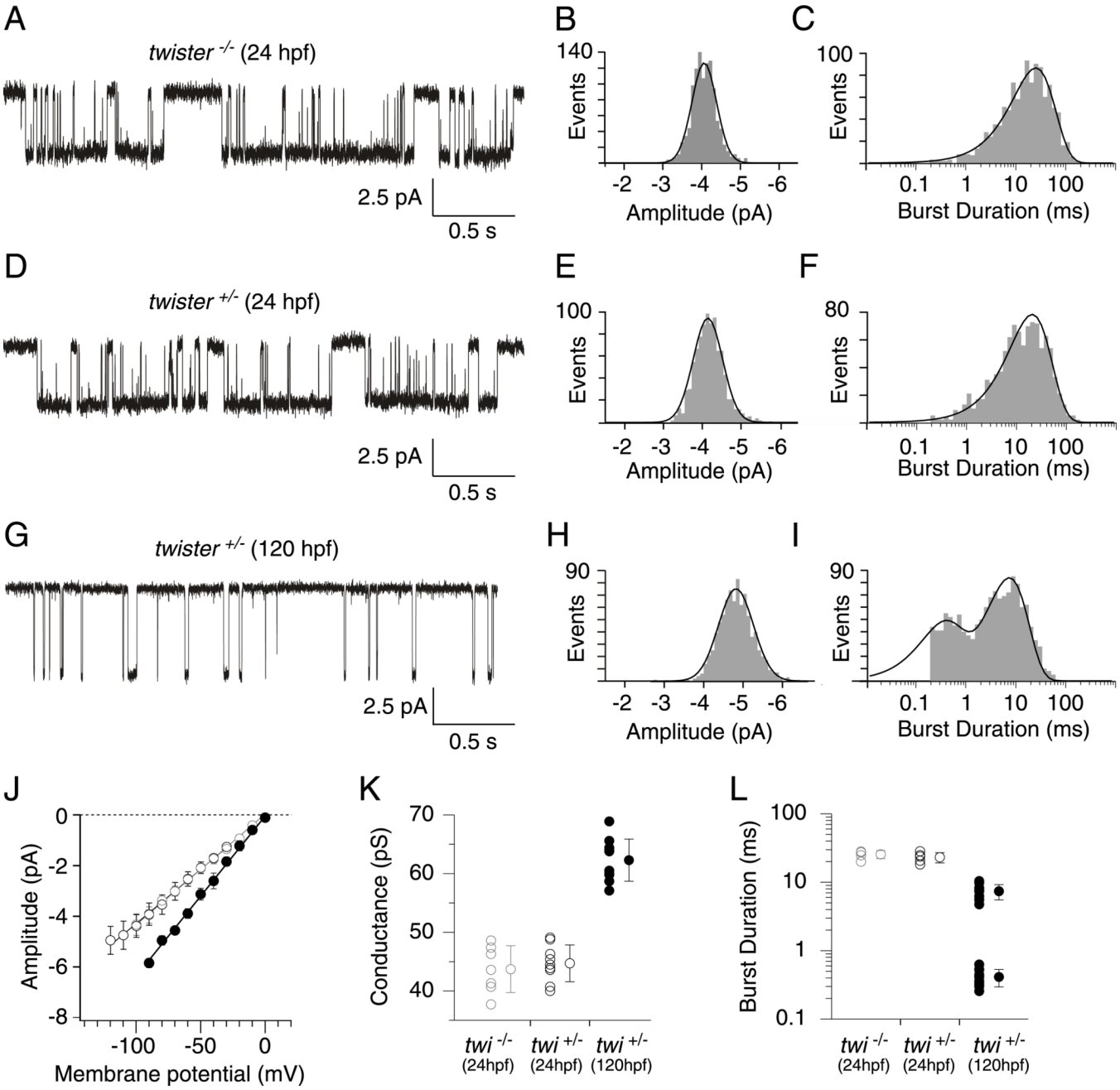

Figure 6. Cell-attached ACh-activated single channel currents from 24 hpf and 120 hpf twister muscle

Sample traces of ACh activated channels in 24 hpf twi$^{-/-}$ (A), 24 hpf twi$^{+/-}$ (D), and 120 hpf twi$^{+/-}$ fish (G). B, E, Amplitude distributions for 24 hpf twi$^{-/-}$ and 24 hpf twi$^{+/-}$ fish fit to single Gaussian distributions. C, F, Example semilog burst duration histograms fit to a single exponential function with time constants corresponding to 24.8 ms (n=904 events) and 23.8 ms (n=970 events) for 24 hpf twi$^{-/-}$ and 24 hpf twi$^{+/-}$ fish respectively. H, Amplitude distribution for 120 hpf twi$^{+/-}$ fish fit with a single Gaussian function. I, Example burst duration histogram for 120 hpf twi$^{+/-}$ fish fit by the sum of two exponential components with time constants corresponding to 0.4 ms and 8.3 ms (n=1170 events). J, Cumulative current-voltage relations comparing 24 hpf twi$^{-/-}$ (grey open circles; n=7), 24

hpf twi$^{+/-}$ (black open circles; n=9) and 120 hpf twi$^{+/-}$ (filled circles; n=10) fish. A range of 17–140 events was used to calculate each point on the current-voltage relationship. K, Mean slope conductance ± SD calculated for 24 hpf twi$^{-/-}$ (43.7± 4.0 pS), 24 hpf twi$^{+/-}$ (44.7± 3.1 pS), and 120 hpf (62.3± 3.6 pS) shown alongside individual slope conductance values. L, The mean burst durations ± SD for 24 hpf twi$^{-/-}$ (25.6 ± 3.4 ms; n=5), 24 hpf twi$^{+/-}$(23.2± 3.9ms; n=5) and 120 hpf twi$^{+/-}$ (7.4 ± 1.9 and 0.41 ± 0.12; n=10) are shown along with the individual cell averages. A range of 376–1170 events was used to calculate the burst duration. All data was obtained using 30 nM ACh.

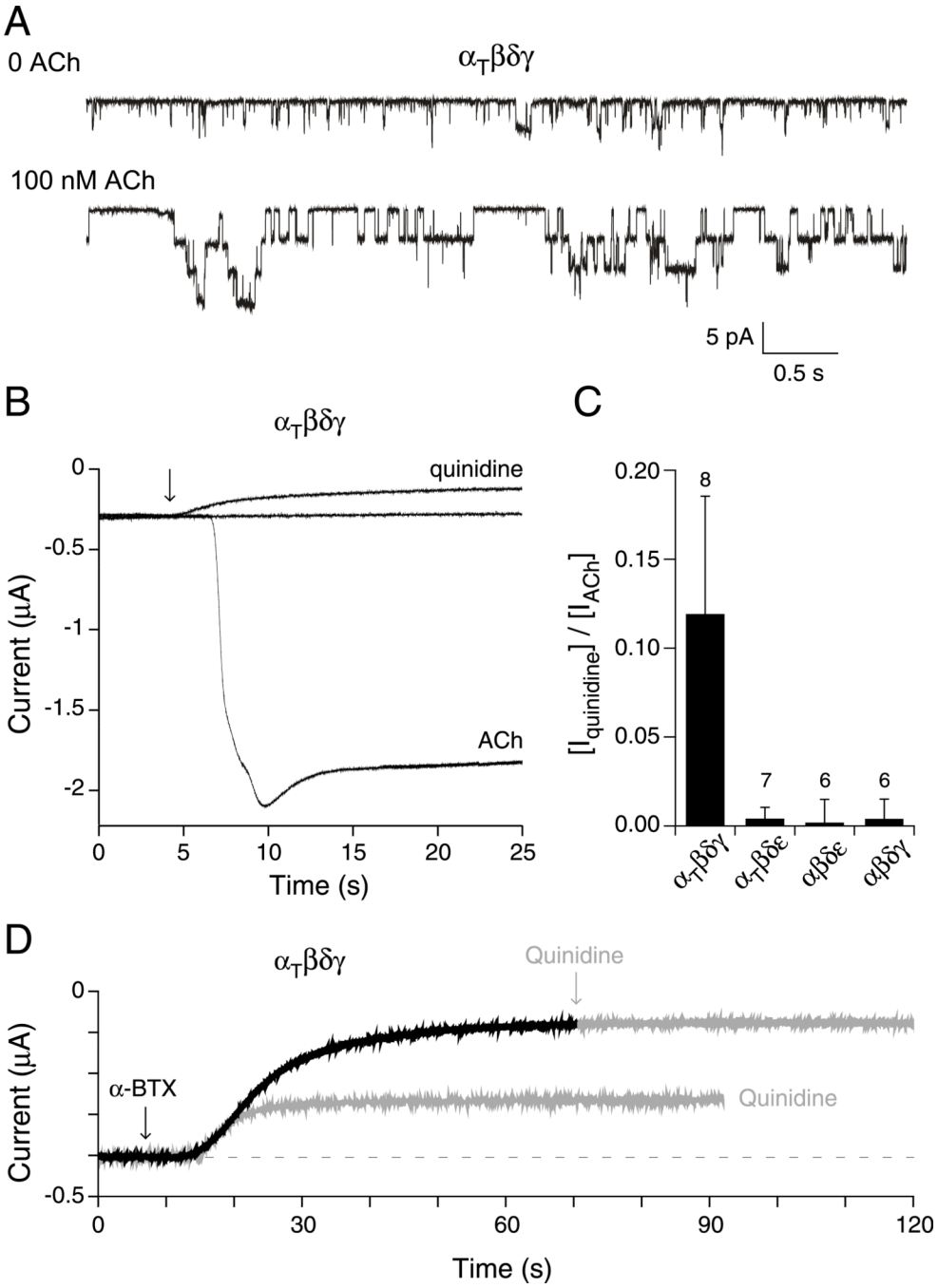

Figure 7. Openings by non-liganded $\alpha_{twi}\beta\delta\gamma$ receptors expressed in *Xenopus* oocytes

A, Outside-out patch recordings of $\alpha_{twi}\beta\delta\gamma$ receptors before (top trace) and after (bottom trace) addition of ACh (n= 6 patches). B, Recordings of macroscopic current in oocytes expressing $\alpha_{twi}\beta\delta\gamma$ and held at −50 mV. Shown are the baseline current in the absence of ACh, the decrease in holding current upon addition of 100 μM quinidine (arrow) and, following wash out of the quinidine, the large inward current that occurred following addition of 300 nM ACh (arrow) to the oocyte. C, Overall comparisons of the effect of quinidine to reduce the holding current in the absence of ACh activation of the different receptor isoforms. The fractional peak current was determined on the basis of reduction in holding current in the presence of 100 μM quinidine relative to total ACh activated current

following washout of quinidine. The mean ± SD are shown and the number of oocytes tested is indicated. (D) Traces from an oocyte expressing $\alpha_{twi}\beta\delta\gamma$ receptors showed decreases in holding current in response to individual application of either 1 μM α-btx (black trace) or 100μM quinidine. The response to the first application of quinidine was allowed to recover before the oocyte was treated with α-btx. Following treatment with α-btx the oocyte showed no response to further application of quinidine (grey arrow).

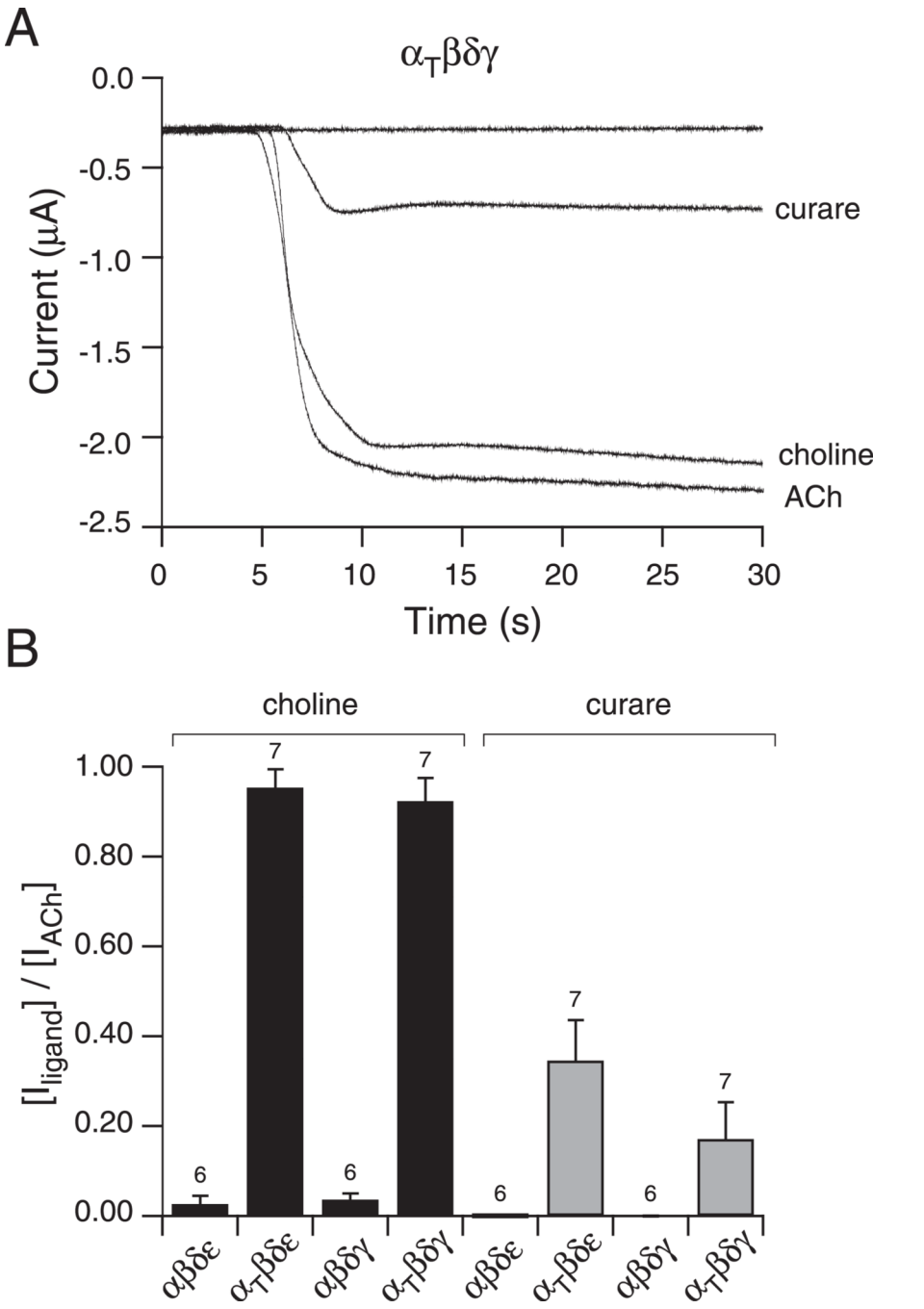

Figure 8. Potency of activation of $\alpha_{twi}\beta\delta\gamma$ receptors by ACh, choline, and curare

A, Recording of macroscopic current in oocytes expressing $\alpha_{twi}\beta\delta\gamma$ and held at −50 mV. Addition of either 10 μM curare, 1 mM choline or 300 nM ACh effectively evoked an inward current. B, Overall comparisons of activation by choline (black) and curare (gray) on each of the different receptor isoforms. The bar graph reflects the mean fractional activation ± SD of peak ACh activated current associated with either curare or choline treatment and the number of oocytes tested is indicated.

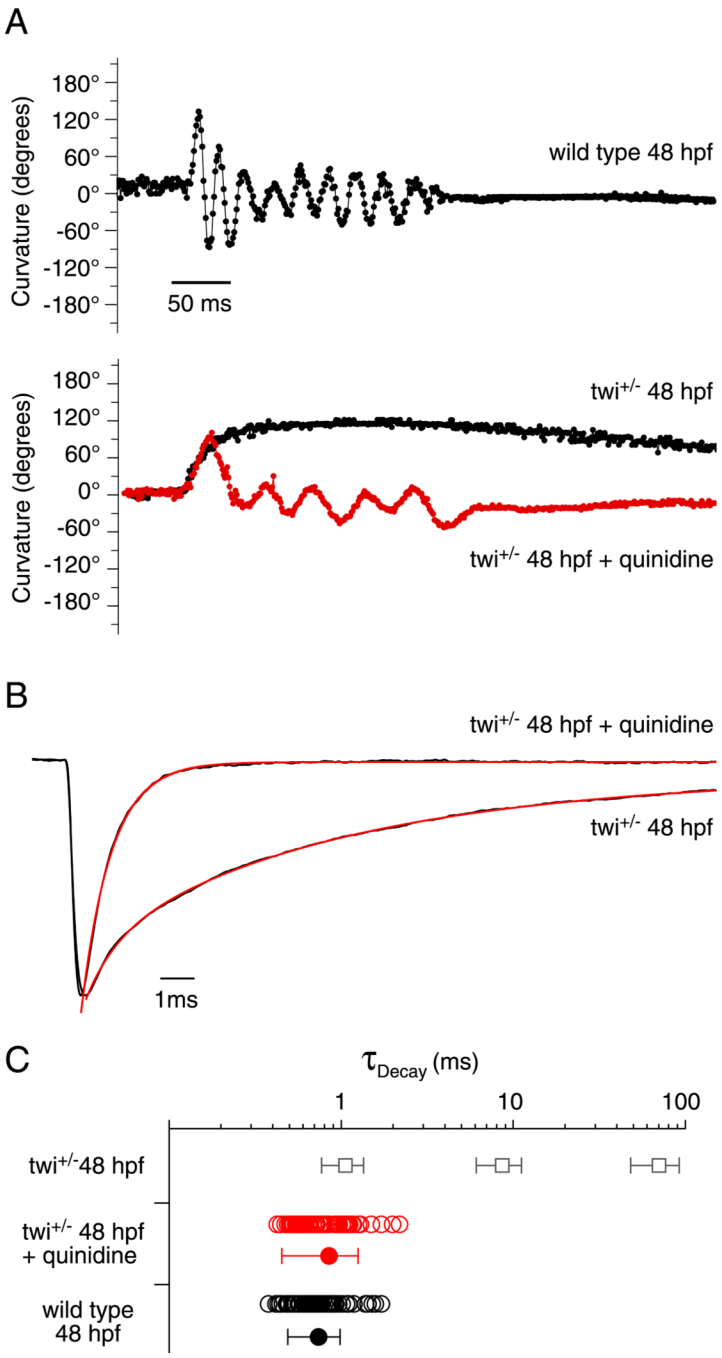

Figure 9. Effect of quinidine on swimming and synaptic current decay

A, Swimming behavior in 48 hpf wild type (top), twi$^{+/-}$ (bottom; black) and twi$^{+/-}$ treated with quinidine (bottom; red). Curvature is measured in 1 ms increments where each point is the sum of the head and tail bend angle relative to the central body axis. B, Normalized mEPC recorded from twi$^{+/-}$ 48 hpf fast muscle cell before and after addition of 10 μM quinidine. Before application the decay was fit by a triple exponential function (red overlay) and after treatment was fit with a single exponential function (red overlay). C, Scatter plot of individual decay time constants for wild type (black open circles; *n*=6 cells; 87 events), and quinidine treated twi$^{+/-}$ (red open circles; *n*=7 cells; 80 events) shown alongside mean ± SD

(filled circles) The mean ± SD for the three $twi^{+/-}$ time constants (Figure 1B) is shown as open squares for comparison.